The effect of pressure on the low energy spin fluctuations in $CeAl_2$ investigated through ^{27}Al nuclear quadrupole resonance and nuclear magnetic resonance measurements

2006 J. Phys.: Condens. Matter 18 10413

(http://iopscience.iop.org/0953-8984/18/46/009)

INSTITUTE OF PHYSICS PUBLISHING JOURNAL OF PHYSICS: CONDENSED MATTER

J. Phys.: Condens. Matter **18** (2006) 10413–10426 doi:10.1088/0953-8984/18/46/009

The effect of pressure on the low energy spin fluctuations in $CeAl_2$ investigated through ^{27}Al nuclear quadrupole resonance and nuclear magnetic resonance measurements

S Tomisawa[1,2], S Wada[1,2], M Ohashi[3] and G Oomi[3]

[1] Department of Material Science, Graduate School of Science and Technology, Kobe University, Nada, Kobe 657-8501, Japan
[2] Department of Physics, Faculty of Science, Kobe University, Nada, Kobe 657-8501, Japan
[3] Department of Physics, Faculty of Science, Kyushu University, Ropponmatsu, Chuo, Fukuoka 810-8560, Japan

Received 29 June 2006, in final form 27 September 2006
Published 3 November 2006
Online at stacks.iop.org/JPhysCM/18/10413

Abstract

To microscopically elucidate the initial evolution of the electronic and magnetic states of a Kondo compound $CeAl_2$ (Néel temperature $T_N \sim 3.8$ K) from the antiferromagnetically ordered state with a spin density wave to a magnetic quantum critical point with the application of pressure P, we have carried out ^{27}Al nuclear quadrupole resonance and magnetic resonance measurements for $P = 0$ and 2.5 GPa. The Knight shift, which is proportional to the uniform susceptibility $\chi(\vec{q} = 0)$, exhibits a rapid increase below ~50 K down to T_N for each pressure, indicating that the sufficiently localized f electron does not directly participate in the formation of the Fermi surface even at $P = 2.5$ GPa. The nuclear spin–lattice relaxation measurements and the analysis lead to the conclusion that the cf hybridized band with a rather large density of states at the Fermi level is formed below an onset temperature above T_N, the value of which increases with the application of pressure. The relaxation rate in the paramagnetic state is dominated by the generalized susceptibility $\chi(\vec{q})$ that has peaks near the antiferromagnetic wavevector $\vec{q} = \vec{Q}_{AF}$ associated with the nesting properties of the Fermi surface of the underlying cf hybridized band. With decreasing temperature, $\chi(\vec{Q}_{AF})$ also exhibits a significant increase larger than that of $\chi(0)$. The finite pressure of 2.5 GPa has the effect of reducing both $\chi(0)$ and $\chi(Q_{AF})$ by about 20% in their magnitudes. Then, changes in the nesting condition with pressure are conjectured to play an important role in depressing the magnetic ordering, in addition to the increase in the extent of mixing J_{cf} between the localized f electrons and conduction electrons.

1. Introduction

The intermetallic Laves-phase compound $CeAl_2$ ($MgCu_2$-type structure) was the focus of various investigations back in the early 1970s, as a convenient laboratory in which the crystal electric field (CEF) splitting [1, 2], Kondo interaction [3], and magnetic ordering [1, 3–5] have a delicate balance in energy. The inelastic neutron scattering experiments revealed the CEF scheme of a Γ_7 (doublet) ground state and two excited states separated from the ground state by $\simeq$100 and $\simeq$180 K, respectively [2]. At ambient pressure, $CeAl_2$ exhibits the antiferromagnetic (AFM) ordering at $T_N \simeq 3.8$ K with a spin density wave (SDW) that is incommensurate with the lattice [6–9]. The electric resistivity exhibits a significant drop below the Kondo temperature $T_K \sim 8$ K [3]. However, many experiments on $CeAl_2$ have been interpreted by placing it not in the local moment regime, but close to the heavy fermion regime with a very narrow cf hybridized band near the Fermi level. The rather large Sommerfeld coefficient $\gamma(0) \sim 0.14$ J mol^{-1} K^{-2} estimated from the electronic specific heat measurements indicates that the system is in a heavy fermion state at low temperatures [10]. An analysis of the neutron Bragg intensity in the AFM state based on a particular assumed modulation configuration indicates an average moment somewhat less than the Γ_7 state value [9]. In fact, previous studies of the magnetization [11] and the neutron diffraction [9] under pressure have revealed continuous depression of T_N and demagnetization of Ce^{3+} magnetic moments.

Then again a few years ago, the system became of intense interest following the discovery of a magnetic quantum phase transition around 3 GPa induced by applying pressure. Electric resistivity measurements reported that the AFM ordering disappears around 3 GPa, where the coefficient of T^2 dependence diverges [12, 13]. The purpose of the present studies is to investigate from a microscopic point of view the initial evolution of the electronic and magnetic states from the AFM ordered state with the SDW to a magnetic quantum critical point with an application of pressure by using ^{27}Al nuclear quadrupole resonance (NQR) and nuclear magnetic resonance (NMR), and to attempt to obtain further insight into its quantum criticality associated with AFM spin fluctuations. The resonance spectra and the data analyses of NQR and NMR are reported in sections 2.1 and 2.2, respectively, with the experimental details. The data and the analysis of the nuclear spin–lattice relaxation rate are reported in sections 2.3. The spin fluctuation character of Ce moments and the evolution with pressure in the AFM order and the paramagnetic (PM) states are reported in sections 3.1 and 3.2, respectively. In section 3.3, we attempt to place in context the implications of our results and make suggestions for further study.

2. Experimental details

Stoichiometric quantities of cerium (99.9% pure) and aluminium (99.99% pure) metals were arc melted in an argon gas atmosphere. An ingot of $CeAl_2$ was grown from a tungsten crucible by using a Czochralski pulling method, and ascertained as single crystal with a single phase of $MgCu_2$-type structure from the Laue pattern. For the NQR and NMR measurements, the single crystals were crushed into powder with grain sizes smaller than the skin depth for the present experimental resonance frequencies. Shown in figure 1 is the dependence of the dc susceptibility χ on temperature T plotted on a log–log scale. The χ data above $\sim$50 K can be satisfactorily reproduced by the Curie–Weiss (CW) law

$$\chi(T) = \chi_0 + g\mu_{\rm eff}^2\mu_{\rm B}^2/3k_{\rm B}(T-\theta), \tag{1}$$

with an effective magnetic moment $\mu_{\rm eff} \simeq 2.57\ \mu_{\rm B}$, a negative Weiss temperature $\theta \simeq -28$ K, and a temperature independent susceptibility $\chi_0 = -1.7 \times 10^{-4}$ emu mol^{-1}. At low temperatures below $\sim$50 K, χ exhibits a rapid increase, and takes a maximum at around 4 K.

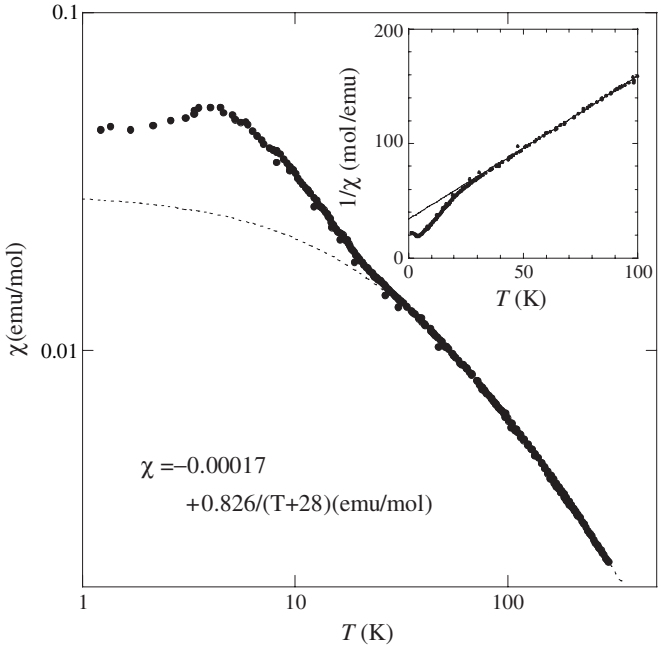

Figure 1. Magnetic susceptibility of $CeAl_2$ at ambient pressure plotted against temperature. The broken curve is the best fit of the Curie–Weiss law to the susceptibility data at high temperatures above 50 K.

2.1. NQR spectra

The NQR and NMR measurements were carried out by using wide band phase-coherent pulsed spectrometers in a temperature range between 1.4 and 200 K. The NQR spectra of ^{27}Al ($I = 5/2$) in zero field were obtained in a frequency sweeping procedure around $2\nu_Q = 1.46$ MHz which corresponds to the $\pm 5/2 \leftrightarrow \pm 3/2$ transition, where ν_Q is the quadrupole frequency [14, 15]. The NMR spectra were observed in a field sweeping procedure at fixed frequencies of 7.00 and 13.55 MHz [14, 16]. Hydrostatic pressures up to 2.5 GPa were applied by using a piston–cylinder pressure cell made of nonmagnetic NiCrAl/BeCu alloys. The Daphne oil 7373 was used as a pressure-transmitting medium.

The ac susceptibility χ_{ac} measured at each of the fixed pressures $P = 0$, 1.0, and 1.2 GPa has two maxima at slightly different temperatures T_{N1} and T_{N2}. Each of the transition temperatures is depressed with increasing pressure as shown in figure 2 by filled and open squares, respectively. The existence of the two peaks in χ_{ac} indicates that the sample at low pressures below at least 1.2 GPa consists of two different types of AFM.

However, the ^{27}Al NQR spectra for the paramagnetic (PM) state have a single resonance line with a rather narrow linewidth as shown in figure 3, indicating that all Al atoms are on a crystallographically equivalent site. With the application of pressure, the NQR frequency slightly shifts toward higher frequencies with a small linewidth broadening. The former is thought to originate from shrinking of the unit-cell volume, and the latter from a small inhomogeneity of pressure within the pressure cell.

At a microscopic level, the AFM ordering of the system is observed in the significant linewidth broadening of the NQR spectrum as shown in figure 4. The onset temperatures of the linewidth broadening at $P = 0$, 1.0, and 2.4 GPa are also plotted in figure 2 with open

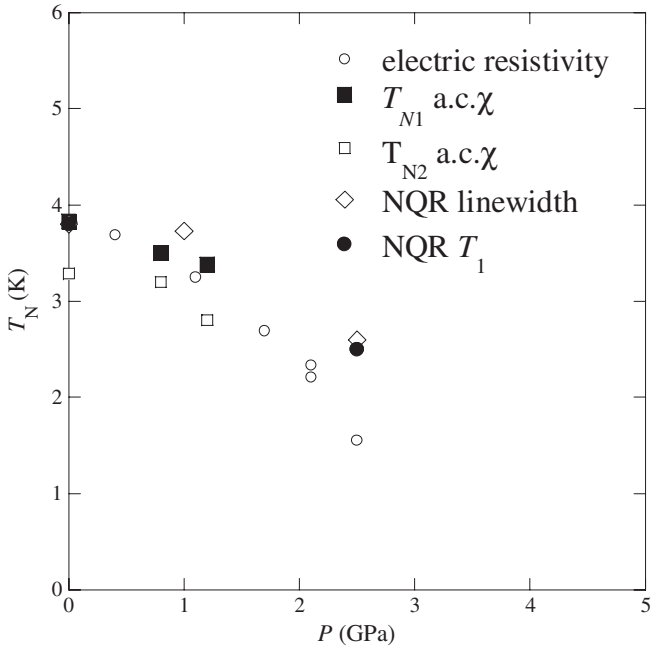

Figure 2. Pressure dependence of the antiferromagnetic ordering temperature T_N of $CeAl_2$ defined at a peak in the electric resistivity (open circles), peaks in the ac susceptibility (filled and open squares), and onsets of NQR linewidth broadening (open diamonds) and the $1/T_1$ drop (filled circles).

diamonds, which are a little bit higher than T_{N1}. As can be seen in figure 4, the NQR spectrum at low pressures below 1.0 GPa has a somewhat complex structure. This feature is considered to be caused by the superposition of two distinct resonance lines originating from each of the two different types of AFM. On the other hand, at a high pressure of 2.4 GPa, the NQR spectrum in the ordered state has a single resonance line. The variation of the NQR spectrum in the shape in the ordered state with pressure can be understood by the fact that the specimen transforms at high pressures into a single phase of AFM with a commensurate wavevector. This feature was evidenced by the neutron diffraction measurements [9]: at low pressures the diffraction peaks with the incommensurate wavevector coexist with the superlattice peaks with the commensurate wavevector, whereas at high pressures above ∼1 GPa the peaks with the incommensurate wavevector disappear.

2.2. NMR spectra

At high magnetic fields, the ^{27}Al NMR spectrum of the powder sample splits into a central line and two satellite pairs. The interval between the first satellite pair yielded a value of the quadrupole frequency $\nu_Q = 0.73$ MHz. The second-order electric quadrupole interaction splits the central line into a maximum at $\theta = \pi/2$ and a shoulder at $\theta = \cos^{-1}\sqrt{5/9}$, where θ is the angle between the applied magnetic field H_{res} and a principal axis of the electric field gradient. By using the conventional spectrum analysis procedure of the central line and the first satellite pair, we deduced the Knight shift $K = (H_0 - H_{res})/H_{res}$, which generally provides information about the uniform static susceptibility $\chi(\vec{q} = 0, \omega = 0, T)$:

$$K(T) = (\gamma_e \gamma_n \hbar^2)^{-1} A_{hf}(q = 0)\chi(0, 0, T), \tag{2}$$

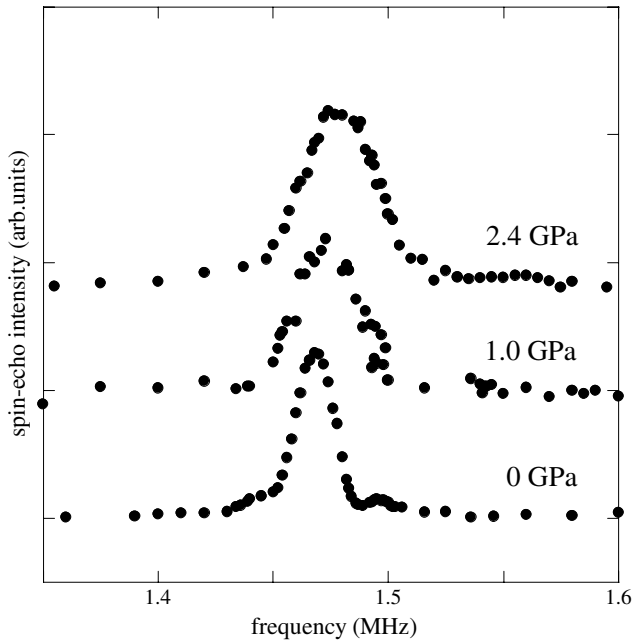

Figure 3. NQR spectra of ^{27}Al in $CeAl_2$ in the paramagnetic state at 4.2 K observed for each of pressures 0, 1.0 and 2.4 GPa.

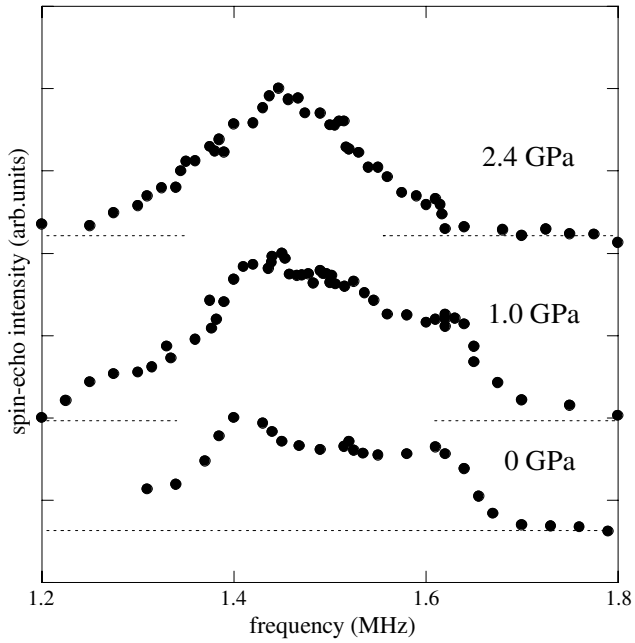

Figure 4. NQR spectra of ^{27}Al in $CeAl_2$ in the antiferromagnetically ordered state at 1.4 K observed for each of the pressures 0, 1.0 and 2.4 GPa.

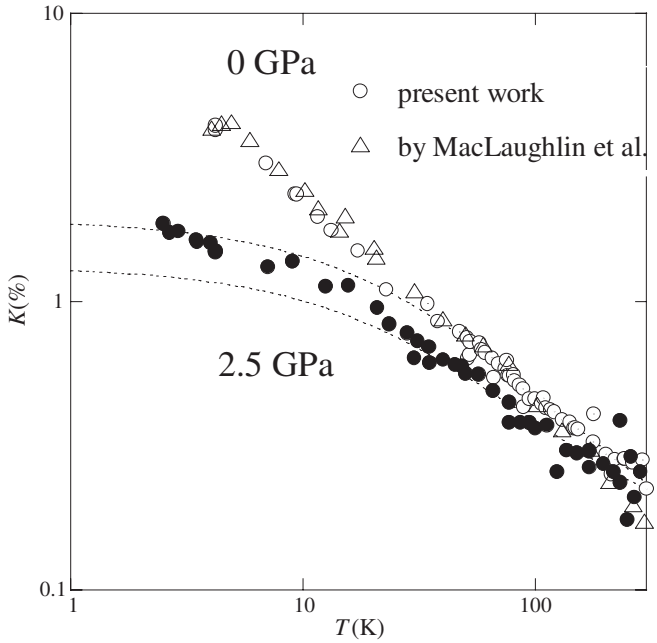

Figure 5. Knight shift of ^{27}Al in the paramagnetic state of $CeAl_2$ plotted against temperature observed at 0 GPa (open circles) and 2.5 GPa (filled circles). The broken curves are the best fit of the Curie–Weiss law with the data above 50 K. The Knight shift at ambient pressure reported by MacLaughlin *et al* [14] is replotted as triangles for comparison.

where $\vec{q}$ is the wavevector, ω the frequency of spin fluctuations, and $A_{\rm hf}(q = 0)/\gamma_{\rm n}\hbar$ the hyperfine field on a given nucleus given by the averaged magnetic moment of neighbouring f electrons induced by $H_{\rm res}$. The temperature dependence of K in the PM state for $P = 0$ and 2.5 GPa is plotted in figure 5 on a log–log scale by open and filled circles, respectively. The K data at ambient pressure previously reported by MacLaughlin *et al* are also plotted as triangles for comparison [14]. K for $P = 0$ exhibits the CW-type increase (broken line) with decreasing temperature down to ∼50 K and a rapid increase at lower temperatures. The values of K for $P = 0$ are replotted in figure 6 against the dc susceptibility with temperature as an implicit parameter. The K versus χ plots are almost on a straight line, and the slope of the line yields an empirical value of the hyperfine field $A_{\rm hf}(q = 0)/\gamma_{\rm n}\hbar \simeq 4.0$ kOe/$\mu_{\rm B}$. MacLaughlin *et al* previously pointed out in their precise K analysis that the ratio of K to χ exhibits a small variation with temperature in a way that is consistent with a simple model of anisotropic hyperfine coupling to the CEF-split Ce ionic states [14]. However, this does not have an essential influence for the conclusions in this study because the increase in the Knight shift and the relaxation rate with temperature are much larger than expected from the change of the hyperfine couplings.

Finite pressure has the effect of reducing both the CW-type K at high temperatures and the rapidly increasing one below ∼50 K as shown in figure 5. The near linear relationship between K and χ makes it possible to establish the $\chi(0, 0, T)$ behaviour at high pressures by measuring K instead of χ, which is difficult to measure at high pressures. The K data at high temperatures above ∼50 K can be fitted by the CW law, with $\mu_{\rm eff} \sim 2.0\mu_{\rm B}$ at $P = 2.5$ GPa, taking the value of the hyperfine field $A_{\rm hf}(q = 0)/\gamma_{\rm n}\hbar \simeq 4.0$ kOe/$\mu_{\rm B}$.

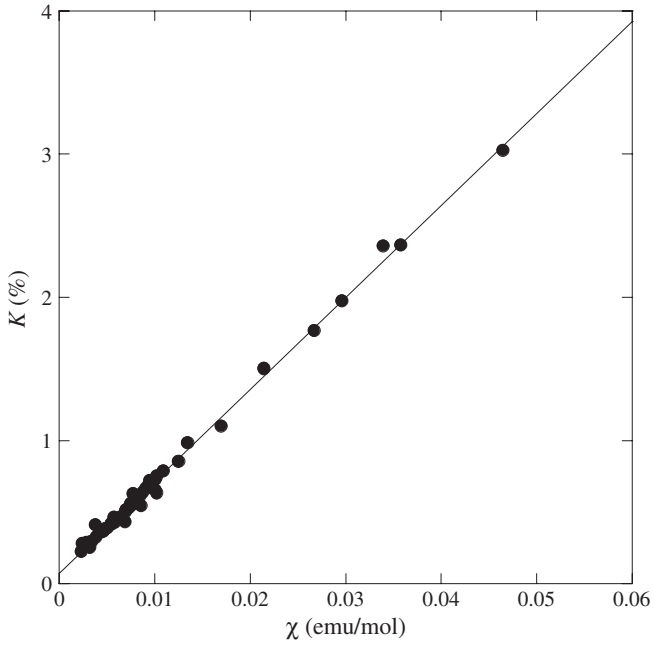

Figure 6. Dependence of the ^{27}Al Knight shift on the uniform magnetic susceptibility at ambient pressure.

2.3. Spin–lattice relaxation rate

Measurements of the nuclear spin–lattice relaxation rate $1/T_1$ reveal the spin fluctuation character from the q averaged dynamical spin susceptibility $\chi(\vec{q}, \omega, T)$,

$$1/T_1 = \frac{k_B \gamma_n T}{2\mu_B^2} \Sigma_q A_{hf}(q)^2 \,\mathrm{Im}\,\chi(\vec{q}, \omega, T)/\omega_0, \tag{3}$$

where ω_0 is the resonance frequency. The ^{27}Al spin–lattice relaxation time T_1 was measured at the peak intensity point of the spectrum by using a single saturation rf-pulse method. The magnetization recovery $M(t)$ at time t after the initial saturation pulse has a multi-exponential behaviour

$$\frac{M(\infty) - M(t)}{M(\infty)} = a_1 e^{-b_1 t/T_1} + a_2 e^{-b_2 t/T_1} + a_3 e^{-b_3 t/T_1}, \tag{4}$$

where $b_1 = 3$, $b_2 = 10$, and $a_3 = 0$ for NQR, and $b_1 = 1$, $b_2 = 6$, and $b_3 = 15$ for NMR. The coefficients a_i depend on the initial saturation condition imposed on all the nuclear spin levels and follow the relation $\sum a_i = 1$. In the low temperature region of the PM state, T_1 was measured by using both the NQR line in zero field and the central line of the NMR spectrum in finite fields. At high temperatures, the NMR line was mainly used to obtain the T_1 values to good accuracy. The magnetization recovery behaviours were satisfactorily reproduced by equation (4). The values of T_1 deduced from the distinct resonance lines of NQR and NMR showed a good agreement. In the AFM state, it was measured by using only the NQR line to exclude the effect of the magnetic field on the nature of spin fluctuations. As shown in figure 7(a), the magnetization recovery behaviour just below T_N was satisfactorily reproduced by equation (4). However, with decreasing temperature well below T_N, the quality of the fit of equation (4) to the recovery data shown in figure 7(b) is somewhat deteriorated, probably due

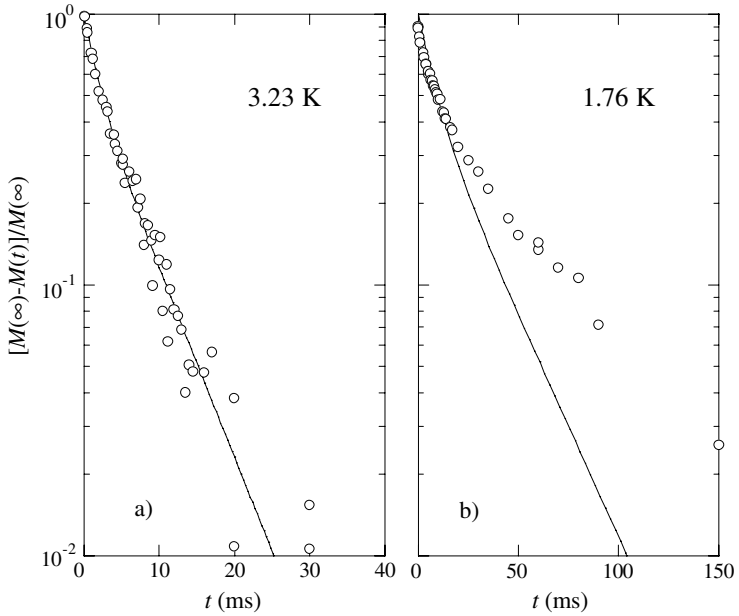

Figure 7. Typical magnetization recoveries $M(t)$ at time t after the application of an initial saturation pulse for the NQR line; a, 3.23 K: b, 1.76 K.

to the distribution of the T_1 values, as previously pointed out by MacLaughlin *et al* [14]. The poor fit to the entire relaxation curves yields a relaxation rate that represents weighted averages over the entire distribution.

The $1/T_1$ data for $P = 0$ and 2.5 GPa are plotted in figure 8 against temperature, as open and filled circles, respectively, on a log–log scale. The data at ambient pressure reported by MacLaughlin *et al* [14] are also plotted in the figure as triangles for comparison. At ambient pressure, there is no significant difference between those $1/T_1$ data in the PM state, even though they were measured independently by using samples prepared separately. The near temperature independent $1/T_1$ at high temperatures exhibits a CW-type increase with decreasing temperature below $\sim$200 K. For $T <\sim 50$ K, it begins to deviate from the CW-type relation, and exhibits the broad maximum around $T^* \sim 10$ K. In the AFM ordered state, $1/T_1$ exhibits a rapid decrease associated with freezing of spin fluctuations and the onset temperature yields an estimate of T_N that is also plotted in figure 2 by filled circles. It is seen in figure 8 that the higher T_N is, the more rapidly $1/T_1$ decreases below T_N. $1/T_1$ observed for $P = 2.5$ GPa exhibits a divergent increase near T_N that is ascribed to the critical slowing down of spin fluctuations. The lack of the $1/T_1$ peak for the data for $P = 0$ could be reasonably explained by the coexistence of the two types of AFM with slightly different T_N, resulting in smearing out of the $1/T_1$ peak.

3. Discussion

The electronic state and low energy magnetic excitations in the PM state of $CeAl_2$ have been rather less studied in comparison with the numerous investigations of the AFM state, and no direct evidence from the macroscopic point of view was found for the Ce moment instability in $\vec{q}$ space or the Kondo moment compensation. The present NMR results for ambient pressure and 2.5 GPa provide further insight into the physics behind the $CeAl_2$ problems.

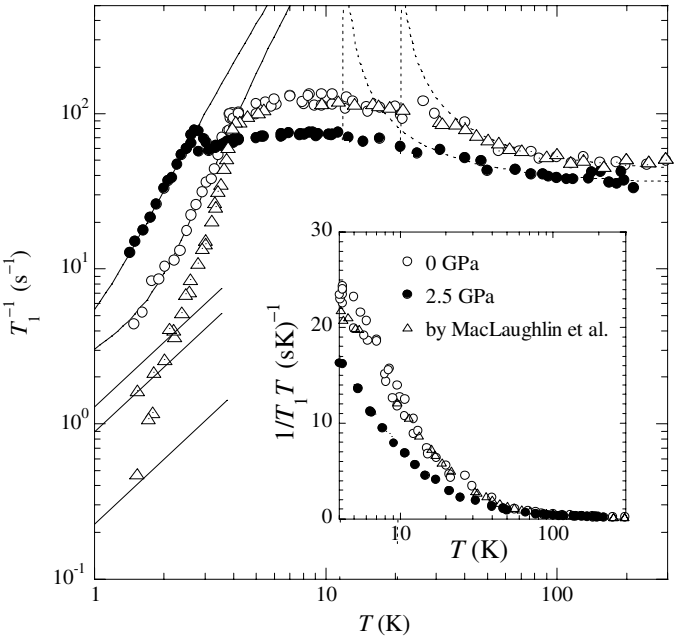

Figure 8. The nuclear spin–lattice relaxation rate $1/T_1$ of ^{27}Al in $CeAl_2$ plotted against temperature observed at 0 GPa (open circles) and 2.5 GPa (filled circles). The $1/T_1$ data at ambient pressure previously reported by MacLaughlin *et al* [14] are replotted as triangles for comparison. Broken curves drawn for a high temperature region are the best fit of the Curie–Weiss law to the data above ∼50 K. Solid curves drawn for a low temperature region are the best fit of the relation $1/T_1 = aT + bT^2e^{-\Delta/k_BT}$ to the data below T_N. Solid lines show the $T_1T = a$ term. The values of $1/T_1$ divided by temperature T in the paramagnetic state above 4.2 K are plotted in the inset as a function of T on a semi-log scale.

The theoretical calculations by Jarlborg *et al* reported that the f bands in the PM state are about 1 eV wide and, although principally above E_F, extend down to accommodate additional electrons [17]. This is consistent with the CW-type behaviour of χ and K at high temperatures with the effective magnetic moment $\mu_{eff} \simeq 2.57\ \mu_B$ near to $2.54\ \mu_B$ for Ce^{3+} ions. The electric resistivity measurements showed the minimum near 10 K, which was the first characterization of $CeAl_2$ as a Kondo compound [3]. A rather large Sommerfeld coefficient $\gamma(0) \sim 0.14$ J mol^{-1} K^{-2} estimated from the specific heat data [10] indicates a heavy fermion state at low temperatures. The analysis of photoemission spectra within the Anderson single-impurity model for $T = 0$ yielded extreme narrowness of the density of the low-lying excitation spectrum. However, χ at low temperatures does not exhibit the saturation behaviour expected for the conventional Kondo lattice, but a rapid increase below ∼50 K down to the Néel temperature as shown in figure 1. These results indicate that $CeAl_2$ would be a heavy electron system if the magnetic ordering below 4 K did not prevent the formation of a coherent Kondo lattice [18].

3.1. Antiferromagnetically ordered state

The suggestion of an AFM ground state of $CeAl_2$ was strengthened by the observation of magnon-like excitations below T_N in the neutron scattering [2]. The $1/T_1$ measurements of ^{27}Al below T_N yielded the thermally activated relaxation rate behaviour $1/T_1 =$

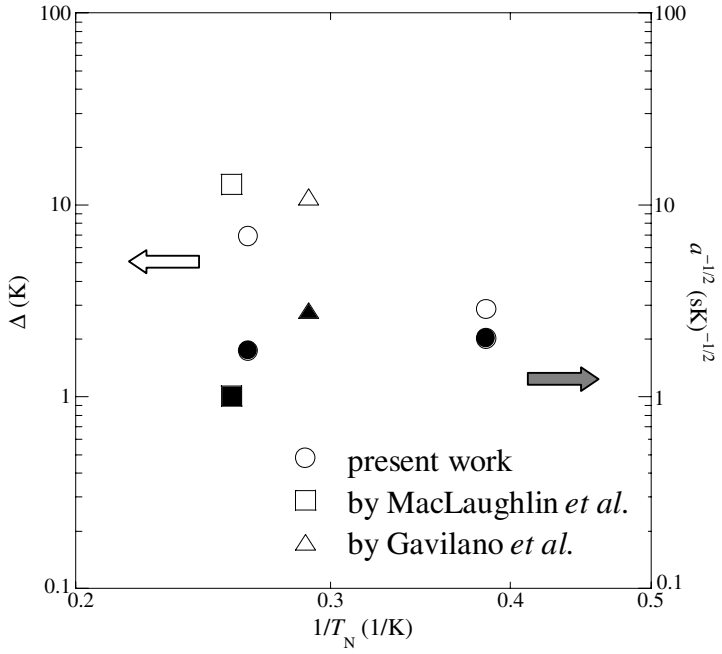

Figure 9. Dependences of the energy gap Δ/k_B of magnon excitations and the square root of the Korringa relaxation term $(T_1T)^{-1/2}$ at low temperatures on the magnetic ordering temperature T_N of $CeAl_2$.

$cT^2e^{-\Delta/k_BT}$ [14, 15] expected for AFM materials where the spin-wave excitations over the energy gap Δ provide the dominant relaxation process [20]. At low temperatures well below T_N, Gavilano *et al* found a different regime where the magnon-driven relaxation is negligible [15]. Instead, a Korringa-like relaxation $1/T_1 = aT$ characterizes the relaxation behaviour that is thought originating from the density of states $N_{cf}(E_F)$ of the narrow cf resonating bands with a rather heavy quasiparticle mass. Solid curves drawn in figure 8 are the best fit of the relation

$$1/T_1 = aT + bT^2e^{-\Delta/k_BT}, \tag{5}$$

with all of the $1/T_1$ data below T_N for $P = 0$ and 2.5 GPa. The values of Δ/k_B and $a^{-1/2}$ are plotted in figure 9 as a function of inverse Néel temperature $1/T_N$, together with the reported values for $P = 0$ given by MacLaughlin *et al* [14] and Gavilano *et al* [15]. The plots at ambient pressure are somewhat scattered. This is probably caused by the poor fit of the recovery curve (equation (4)) to the entire relaxation data and/or the slightly different sample qualities in the ordered state. However, it is still worth noting that with the decrease of T_N, $a^{-1/2}$ ($\propto N_{cf}(E_F)$) of the present study (filled circles) tends to increase whereas the energy gap of magnon excitations Δ/k_B (open circles) exhibits a significant decrease. This is considered to be consistent with the AFM order accompanied by the SDW that is related to nesting features in the underlying FS.

The self-consistent band calculations indicated that in the AFM phase of $CeAl_2$, the 4f levels occupied by about one electron get narrower in energy, and the sufficiently localized f electron does not participate in the formation of the FS [17]. Instead, the itinerant electrons like those of $LaAl_2$ were conjectured to set up the FS, whose nesting properties lead to peaks in the generalized susceptibility $\chi(\vec{q})$ and to the SDW ordering with the wavevector $\vec{q} \neq 0$. Then

the peaks in $\chi(\vec{q})$ and the SDW ordering are considered to be significantly depressed with the application of pressure or chemical pressure. As can be seen in figure 8, this actually appears as the decrease in the $1/T_1$ values just above T_N with pressure, since $1/T_1$ in the PM state is dominated by $\chi(\vec{q}, 0, T)$ with finite wavevector $\vec{q}$ far from $\vec{q} = 0$ as described below.

The straight lines drawn for a low temperature region in figure 8 represent the first $1/T_1 = aT$ term in equation (5). The most important feature is that the value of $1/T_1$ given by extrapolating each of the lines exceeds the actual $1/T_1$ values at a high temperature. This indicates that the conduction band with $N_{cf}(E_F)$ is formed at a rather low temperature associated with the coherent Kondo scattering. In other words, the cf hybridized band coexists with the sufficiently localized f band at low temperatures.

3.2. Paramagnetic state

We now focus our interest on the low energy fluctuations of the Ce moment in the PM phase of $CeAl_2$. In the previous analysis of the characteristic T_1 behaviour in the PM phase by MacLaughlin *et al* [14], an effective spin correlation time τ_{eff} is defined as proportional to $1/T_1T$ and a simple theory, which does not consider the $\vec{q}$ dependence of $\chi(\vec{q}, \omega, T)$, suggests the onset of spatial short range magnetic ordering at low temperatures below ~100 K, but the nature of this order is uncertain. A few years later, Thuan *et al* proposed a different model; $1/T_1$ on the Al site measures the generalized susceptibility $\chi_s(\vec{q}, \omega, T)$ of s electrons, which is indirectly enhanced by the 4f electrons via the cf exchange interactions [19]. However, from the theoretical point of view of this model, $1/T_1T$ at high temperatures tends to its pure s band value, $1/(T_1T)_s \propto N_s(E_F)^2$. This is not the case for $CeAl_2$ in this study because at high temperatures above ~100 K, $1/T_1$ is nearly constant and the magnetic susceptibility χ can be well fitted by the CW law without temperature independent contributions.

Our explanation of the characteristic temperature dependence of T_1 is clearly different from previous analyses. As shown in figure 6, the Knight shift $K(T)$ is directly proportional to the uniform susceptibility $\chi(T)$. The $1/T_1T$ data for the PM state are replotted in figure 10 against K with temperature as an implicit parameter. Each of the plots for $P = 0$ and 2.5 GPa are not on any straight lines. Therefore, $1/T_1T$ cannot be scaled by the uniform susceptibility $\chi(0, 0, T)$, indicating that the relaxation of ^{27}Al is dominated by the generalized susceptibility $\chi(\vec{q}, \omega, T)$ with a finite wavevector $\vec{q}$ (most probably the AFM wavevector $\vec{Q}_{AF}$). In other words, the characteristics of $1/T_1$ in the PM state shown in figure 8 just correspond to those of $T\chi(\vec{Q}_{AF}, 0, T)$ associated with the AFM spin fluctuations of strongly correlated f electrons. As shown in the inset of figure 8, $1/T_1T$ also exhibits a large increase at low temperatures for each of the pressures $P = 0$ and 2.5 GPa. Figure 10 indicates that the increasing rate of the staggered susceptibility is much larger than that of the uniform susceptibility.

The $1/T_1$ data at high temperatures above ~200 K are well reproduced by the CW relation (broken curve drawn in figure 8)

$$1/T_1T = c/(T - T_N(\vec{q} = \vec{Q}_{AF})), \tag{6}$$

with $c = 42$ s^{-1} and $T_N(\vec{q} = \vec{Q}_{AF}) = 20$ K for $P = 0$, and $c = 35$ s^{-1} and $T_N(\vec{q} = \vec{Q}_{AF}) = 12$ K for $P = 2.5$ GPa. Here, c is directly proportional to the staggered susceptibility associated with the conduction cf resonance band. The application of pressure 2.5 GPa has the effect of reducing the effective magnetic moment by about 20% for both the uniform and the staggered susceptibilities. A remarkable difference in the pressure effect emerged in the Weiss temperatures: $T_N(\vec{q} = \vec{Q}_{AF})$ for the staggered susceptibility is greatly depressed as described above, in contrast with the near pressure independent behaviour of θ for the uniform susceptibility.

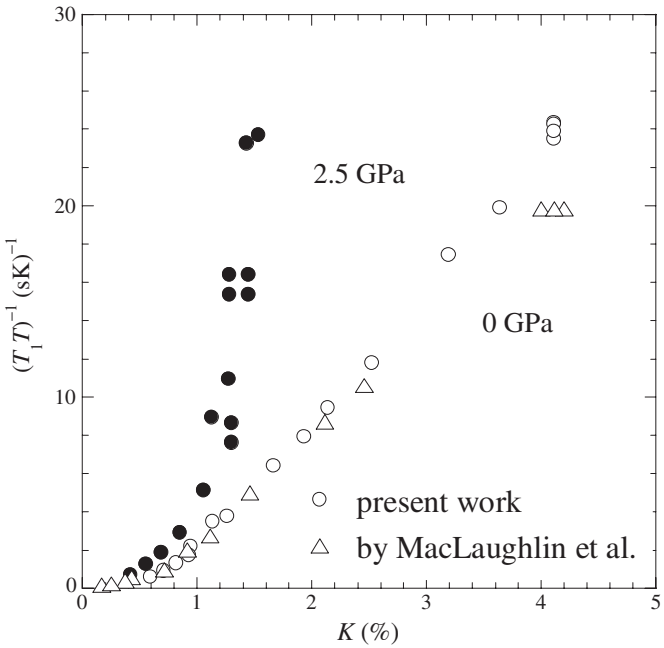

Figure 10. The $1/T_1T$ versus K plots of ^{27}Al in the paramagnetic state of $CeAl_2$ for each of the pressures $P = 0$ and 2.5 GPa. The plots for the $1/T_1T$ reported by MacLaughlin *et al* [14] are also shown as triangles for comparison.

With decreasing temperature below ∼50 K, instead of a divergent increase of $1/T_1$ near $T_N(\vec{q} = \vec{Q}_{AF})$ expected from the CW relation at high temperatures, it begins to deviate from the relation and takes a broad maximum around T^* above T_N; ∼10 K for $P = 0$ and ∼8 K for $P = 2.5$ GPa. The so-called 'spin-gap' behaviour of $1/T_1$ has been observed in many of the high T_c cuprates and heavy fermion compounds, and is usually explained by relating it to an unconventional metal–insulator transition, or by taking the Fermi liquid point of view and taking the itinerant AFM spin fluctuations into account.

However, this is not the case for the $CeAl_2$ system, since the f electrons are sufficiently localized and the itinerant electrons are considered to set up the underlying FS, whose nesting properties give rise to the SDW order. Miyake *et al* developed the mode–mode coupling theory for the spin fluctuations in the normal state of high T_c cuprates on the basis of the itinerant–localized duality picture of nested FS of quasiparticles. They indicated that in the low temperature region where the itinerant spin fluctuation dominates, the nested spin fluctuations decrease on decreasing temperature or approaching the perfect nesting, while the profile is sharpened, leading to the 'spin-gap' behaviour of the specific heat, the uniform susceptibility, and optical conductivity [21]. They also pointed out that the 'spin-gap' behaviour of $1/T_1$ arises from a more delicate balance of 'nested' spin fluctuations. In the PM state of $CeAl_2$ near T_N, the application of pressure of 2.5 GPa results in an increase of $N_{cf}(E_F)$ and a decrease of $\chi(\vec{Q}_{AF})$. These feature suggest that the peak around $\vec{Q}_{AF}$ in the generalized susceptibility, originating from the nesting properties of the FS, is depressed on applying pressure.

3.3. Implication and suggestion of NMR results

The value of T_N decreases with pressure as shown in figure 2, and the AFM ordering is considered to be completely suppressed near 3 GPa where the coefficient of the T^2 dependent

electric resistivity exhibits the divergent increase [12, 13]. The application of pressure on Ce-based compounds generally increases the extent of mixing J_{cf} between the localized f electrons and conduction electrons, resulting in the decrease of the RKKY interactions and the increase of the Kondo interactions. Most of the pressure-induced magnetic quantum critical behaviour has been explained by the competition between the RKKY and Kondo interactions based on the schematic T–$J_{cf}N(E_F)$ phase diagram proposed by Doniach [22]. However, the present NMR investigation of $CeAl_2$ at a high pressure of 2.5 GPa provides evidence that the f electrons are still well localized down to low temperatures, though the magnitude of the moment is somewhat reduced. Thus, the change of the nesting condition of the FS of the underlying conduction band is considered to also play an important role in depressing the magnetic ordering, in addition to the increase in the extent of mixing J_{cf}. Further development of this work, particularly the measurements near 3 GPa, will aim at clarifying the dynamic processes in this system.

4. Conclusion

We have carried out ^{27}Al NQR and NMR studies for $P = 0$ and 2.5 GPa to microscopically elucidate the initial evolution of the electronic and magnetic states of $CeAl_2$ from the AFM ordered state with the SDW to a magnetic quantum critical point with the application of pressure. The Knight shift that is proportional to $\chi(\vec{q} = 0)$ exhibits a significant increase below $\sim$50 K down to T_N for each of the pressures, indicating that the sufficiently localized f electron even for $P = 2.5$ GPa does not participate in the formation of the FS. The $1/T_1$ measurements and the analysis in this study lead to the conclusion that the cf resonance band with a rather large $N_{cf}(E_F)$ is formed below an onset temperature above T_N, the value of which increases with pressure. $1/T_1$ in the PM state is dominated by the generalized susceptibility $\chi(\vec{q})$, which has peaks near $\vec{q} = \vec{Q}_{AF}$ associated with the nesting properties of the Fermi surface of the underlying cf hybridized band. With decreasing temperature, $\chi(\vec{Q}_{AF})$ also exhibits a larger increase than $\chi(0)$ does. The application of the pressure 2.5 GPa has the effect of reducing both $\chi(0)$ and $\chi(Q_{AF})$ by about 20% in their magnitudes. Then, changes in the nesting condition with pressure, in addition to the increase in the extent of mixing J_{cf}, are conjectured to play an important role in depressing the magnetic ordering.

Acknowledgments

The authors wish to thank Dr T Mito for help in the high pressure NMR experiments. This work was partially supported by a Grant-in-Aid for Scientific Research from the Ministry of Education, Science and Culture of Japan, Grant No 16340105.

References

[1] Walker E, Purwins H-G, Landolt M and Hulliger F 1973 *J. Less-Common Met.* **33** 203 and references therein
[2] Loewenhaupt M and Steglich F 1977 *Physica (Utrecht)* **86–88B** 187
[3] Buschow K H J and van Daal H J 1969 *Phys. Rev. Lett.* **23** 408
[4] Swift W M and Wallance W E 1969 *J. Phys. Chem. Solids* **29** 2053
[5] Hill R W and Machado da Silva J M 1969 *Phys. Lett.* A **30** 13
[6] Barbara B, Boucherle J X, Buevoz J L, Rossignol M F and Schweizer J 1977 *Solid State Commun.* **24** 481
[7] Shapiro S M, Gurewitz E, Parks R D and Kupferberg L C 1979 *Phys. Rev. Lett.* **43** 1748
[8] Osborn R, Loewenhaupt M, Rainford B D and Stirling W G 1987 *J. Magn. Magn. Mater.* **63/64** 70
[9] Barbara B, Rossignol M F, Boucherle J X and Vetter C 1980 *Phys. Rev. Lett.* **45** 938
[10] Steglich F, Bredi C D, Loewenhaupt M and Schotte K D 1979 *J. Physique Coll.* **40** C5 301
[11] Croft M C and Jayaraman A 1979 *Phys. Rev.* B **20** 2073

[12] Braithwaite D 2002 *PhD Thesis* Université Joseph-Fourier Grenoble I
[13] Oomi G, Ohashi M, Uwatoko Y, Satoh I and Komatsubara T 2005 *Physica* B **359–361** 2073
[14] MacLaughlin D E, Pëna O and Lysak M 1981 *Phys. Rev.* B **23** 1039
[15] Gavilano J L, Hunziker J, Hudak O, Sleator T, Hulliger F and Ott H R 1993 *Phys. Rev.* B **47** 1993
[16] Silbernagel B G, Jaccarino V, Pincus P and Wernick J H 1968 *Phys. Rev. Lett.* **20** 1091
[17] Jarlborg T and Freeman A J 1986 *J. Magn. Magn. Mater.* **60** 291
[18] Patthey F, Schneider W-D and Bear Y 1987 *Phys. Rev.* B **35** 5903
[19] Thuan N, Lores L C and Coqblin B 1986 *Phys. Rev.* B **33** 4522
[20] Jaccarino V 1965 *Magnetism II* ed G Rado and H Suhl (New York: Academic) p 307
[21] Miyake K and Narikiyo O 1994 *J. Phys. Soc. Japan* **63** 3821
[22] Doniach S 1977 *Valence Instability and Related Narrow Band Phenomena* ed R D Parks (New York: Plenum)